Journal of Materials Chemistry A

Accepted Manuscript

ROYAL SOCIETY OF CHEMISTRY

www.rsc.org/materialsA

Journal Name

RSCPublishing

ARTICLE

High-Performance Si-based 3D Cu Nanostructured Electrode Assembly for Rechargeable Lithium Batteries

Ning Wang, Tao Hang*, Huiqin Ling, Anmin Hu, Ming Li

Cite this: DOI: 10.1039/x0xx00000x

Received 00th January 2012,
Accepted 00th January 2012

DOI: 10.1039/x0xx00000x

www.rsc.org/

In this work, we report the synthesis of Si/Cu nanocone-array (NCA) electrode via a facile ambient electrodeposition method with subsequent magnetron sputtering deposition. The close connection between Cu NCA and silicon layer facilitates the charge transfer in the system and supports a binder-free technique of preparing lithium ion battery (LIB) anodes. The void spaces between Si cylinders allow not only greater alleviation of the strain caused by the Si expansion during lithiation but also a significantly enhanced rate performance due to the increasing electrode/electrolyte contact area, and shortening path lengths for electronic and Li^+ transport. Such engineered electrodes exhibit a long cycle life up to 2000 cycles and can be very promising for high-performance anode applications.

Introduction

With the ever-accelerating pace of life, there is an increasing demand in developing rechargeable lithium-ion batteries (LIBs) with both higher energy densities and power densities for application in powering portable electronic devices and electric vehicles.[1-3] Silicon (Si) is widely regarded as a very promising anode material for high-performance Li-ion batteries, possessing an ultrahigh specific capacity of ~3580 mAh g^{-1} (in the form of $Li_{3.75}Si$), which is much higher than that of commercialized graphite anodes (372 mAh g^{-1}).[4] Furthermore, Si is the second most abundant element in the earth's crust and has potential for low-cost exploration and production.[5] However, during charging, i.e. lithiation step, lithium/silicon alloying yields very high volume expansion, up to 300%, while contraction during discharging, [6,7] which induces mechanical disintegration, thus very poor cycle life. Comparing with other energy storage devices, LIBs possess considerable energy densities, but relatively low power densities. Thus, improving the power densities and cycle performance of alternative materials is of crucial importance. In response to this situation, nanoelectrodes have emerged as an attractive solution. Firstly, nanostructured Si anodes for LIBs are more resistant to fracture than larger Si structures, because the total elastic energy stored in a small nanostructure during deformation isn't sufficient to drive crack initiation and propagation.[6] Secondly, nanoelectrodes can increase electrode/electrolyte contact area, and shorten path lengths for electronic and Li^+ transport.[8, 9]

To avert the limitation of conventional silicon-based anodes, major efforts have been focused on the development of novel nano-architectured electrode design of silicon, such as nanowires,[10-13] 3D nano-current collector electrode,[14-16] hollow nanospheres,[17] core–shell nanofibers,[18] yolk-shell structured Si composites,[19] silicon nanotubes,[20,21] mesoporous silicon.[22] The aim of all these nanostructured designs is to engineer empty space between Si nanoparticles, which shows both improved cyclability and rate performance.

The use of nanoarchitectures is a promising approach for realizing high performance electrodes with both higher energy densities and rate performance. These nanostructured designs have greatly increased the cycle life of silicon anodes to up to a few hundred cycles. However, the complexity of the fabrication processes and the high cost of 3D nanoarchitectures have hindered mass production and practical applications. For example, to fabricate porous Si, typically, SiO_2 was used as templates by partially oxidizing Si or by hydrolysis of tetraethyl orthosilicate (TEOS), followed with carbon or silicon coating and etching of SiO_2 using HF,[17,23] the synthesis process of which is complicated and not eco-friendly. To obtain functional bare 3D nanoarchitectures, template methods are needed which involve several steps including fabrication and removal of templates.[24] It is thus essential to develop simple and inexpensive fabrication methods for 3D nanostructures that may be used for low cost commercial batteries.

Owing to the above obstacles, it seems that practical electrode manufacture would require a simpler electrode fabrication process compatible with the use of low-cost and high-efficiency materials. Moreover, the core idea is to design free volume around active material, allowing for expansion without breaking.[14] Keeping such needs in mind, we selected 3D nanostructured copper current collectors and chose Si as an

active material. Recently, our group successfully developed Cu nanocone-array (NCA) material at ambient temperature by a facile one-step electrodeposition method, the manufacturing process of which is low-cost, efficient and non-toxic.[25] Here we report an electrode comprised of vertically aligned Cu NCA decorated with silicon particles (Si/Cu NCA). This type of 3D nanostructure has several advantages. i) The conductive Cu core was directly grown from the current collector forming a 3D current collector substrate so that each particle of active material has its "own" current collector, which allows for more contact area and effective electron conduction to enhance the battery's rate capability. ii) The cone-shaped current collector was deeply wedged into the active material which facilitates charge and thermal transfer in the electrode system. iii) Si/Cu NCA electrode incorporated empty space for effective accommodation of strain to improve the cycle performance. iv) The Si/Cu NCA structure is a binder-free and conductive additive-free technique for preparing electrodes for LIBs.

Experimental Section

Material synthesis

Cu nanocone-array (NCA) growth: Cu NCA was grown on thick copper foil through a one-step electrodeposition method at ambient temperature. A Cu plate was used as the anodic electrode while a copper foil was used as the cathodic electrode for Cu NCA deposition. Firstly, these Cu foils were pretreated by electrochemically degreasing, 20% H_2SO_4 cleaning, and then coated with insulating tapes, rendering an exposed area of 1 cm × 1 cm. Secondly, the copper foil was immersed into the simple electrodeposition solution, which was composed of $CuSO_4$•$5H_2O$ (providing Cu^{2+} ions) 0.25 mol L^{-1}, H_3BO_3 (pH buffer) 0.3 mol L^{-1} and crystal modifier Janus Green B (JGB) 0-0.2 g L^{-1}. The pH value was adjusted to 3.0 by addition of 10wt% H_2SO_4 solution. The electrodeposition time was only 3 min.

Si coating: Amorphous Si (contain a small amount of crystal Si) was performed by radio frequency magnetron sputtering in a SPC-350 (ANELVA, Japan) magnetron sputtering system. The target used for sputtering was 7.5 cm in diameter. The distance between the substrate and the target was fixed at 5 cm. The copper foil with Cu NCA was directly exposed to the target, with no bias voltage applied on the substrate. Si sputtering was then carried out in Ar atmosphere for 50 min, 70 min and 90 min, respectively with a working pressure of 0.6 Pa and sputtering power of 40 W. Copper foil without Cu NCA was also sputtered for 70 min as a control sample.

Structural Characterizations

The electrodes were characterized using a field emission scanning electron microscope (FE-SEM, FEI SIRION200/INCA OXFORD, FEI, U.S.A), a field emission transmission electron microscope (FE-TEM, JEM 2100F, JEOL, Japan), and Raman spectrometer (LabRam HR, Horiba JobinYvon, France). The elemental compositions of deposits were studied by Energy Dispersive X-ray Detector (EDX). X-ray diffraction patterns were recorded from 40° to 110°, using a Rigaku D/MAX-IIIA X-ray polycrystalline diffractometer with Cu K_α radiation (λ=0.15418 nm).

Electrochemical Characterizations

For the evaluation of the electrochemical properties of such prepared electrodes, a three-electrode electrochemical cell was fabricated in a high-purity argon filled glove box. A solution of 1.0 M $LiPF_6$ in a solvent mixture of ethylene carbonate (EC) and dimethyl carbonate (DMC) (1:1 vol%) were used as an electrolyte and pure Li metal foils as both reference electrode and counter electrode. The galvanostatic discharge-charge cycling was carried out with cut-off voltages of 0.01 V and 1.6 V by using a multichannel battery tester (Neware, BTS-610) at 25 °C. Cyclic voltammetry was performed at a scanning rate of 0.1 mV s^{-1} via an electrochemical workstation (CHI660E). The loading mass of Si was determined by measuring the thickness of the sputtered silicon on a flat Si (100) wafer placed next to the Cu foils. A Bruker Dektak XT stylus profiler was used for Si film thickness. Due to the uniform deposition, the specific area amount of Si sputtered onto the Cu NCA should be the same as that in the flat area next to them. Here we use the nominal thickness (i.e. the thickness equivalent to that on a flat Si wafer) to calculate the quantity of Si deposition on Cu NCA. For a Si layer with nominal thickness H and density of 2.33 g cm^{-3}, the mass per electrode (~1×1 cm^2) can be calculated as:

$$Si\ Mass = (1 \times 1 cm^2) \times 2.33\ g\ cm^{-3} \times H$$

The nominal thicknesses H for 50CuSi, 70CuSi and 90CuSi are 209 nm, 319 nm, and 387 nm, respectively, and thus, the corresponding Si masses are 49.68 μg, 74.34 μg, and 90.12 μg.

Results and discussion

Figure 1 illustrates a typical preparation procedure of the electrode. Firstly, the Cu NCA was grown by directly electroplating on foil at ambient temperature in a few minutes (Figure 1b). The bath solution included several common chemical reagents, like $CuSO_4$•$5H_2O$ (providing Cu^{2+} ions), H_3BO_3 (pH buffer) and Janus Green B (JGB).The equipment used for the fabrication of the nanostructured Cu current collector is very simple (Figure 1a), and is scalable to manufacturing levels of production. Secondly, a variable thickness of silicon layer was deposited on top of the Cu NCA by magnetron sputtering deposition technique (Figure 1c). Magnetron sputtering allows the direct fabrication of a perfect junction between metal and silicon, despite no binder, with Cu NCA acting as current collector as well as the structural support and inactive confining buffer.

Scanning electron microscopy (SEM) images are shown to characterize the morphologies of the as-grown Cu NCA and Si/Cu NCA structures (Figure 2 a–f). Figure 2a and b are the low-magnification and high-magnification SEM images of the Cu NCA, which were electrodeposited for only 3 min onto the Cu substrate in a plating bath. The morphology and size of the nanocones are relatively homogeneous and regular. The bases of the cones show an average diameter of around 200 nm

whereas the mean height of the cones is 400-500 nm. The surface of the cones is very rough, thus, it is expected to have good adhesion with the Si layer. Such novel and robust Cu NCA structure, without utilization and emission of toxic substances in the fabrication process, is very promising and worthwhile to be reported here as 3D current collector of Li-ion batteries. Figure 2 c-f shows SEM images of as-prepared Si/Cu NCA structures for four different deposition times ranging from 25 min to 90 min. The Cu signal and Si signal are both detected in the EDX spectrum (Figure S1). Overall, all deposition times give good coverage on the Cu NCA. At the time of 25 min, the Cu cone morphology with sharp tips is still retained, and the core-shell structure is faintly visible. When the deposition time comes to 50 min, the sharp tips are invisible, while a large number of voids exist between Si/Cu NCA structures, which facilitate full contact between electrolyte and electrode. When increasing the deposition time to 70 min, the Si layer further thickens. With an even longer deposition time, the Si grain on the cones grows bigger, and nearly devours the nanogap between Cu NCA.

The morphology and composition of Si/Cu NCA structures were characterized by transmission electron microscopy (TEM). Figure 3a is the low magnification TEM image, where the uniformity and core-shell bilayer of Si/Cu NCA structures are evident and the thickness of the composites is approximately 800 nm (about 300 nm more than the height of Cu cones). Figure 3b shows the high magnification TEM image of an individual Si/Cu NCA structure that possesses a black core and a gray feather-like shell. The selected area electron diffraction pattern (SAED; Figure 3c) recorded over a single cone, clearly exhibiting both twin diffraction spots of the Cu core and the dispersed amorphous diffraction pattern of the Si shell. A high-resolution TEM image (HRTEM; Figure 3d) was taken at the interface of the black core and gray shell, showing the close binding of Si layer and Cu cone. The crystalline planes at the black core with a d-spacing value of 0.21 nm indicate a Cu (111) plane. However, no pronounced crystalline plane is observed in the gray shell, implying a major amorphous material phase. This is consistent with the X-ray diffraction results which also show no Si crystal peaks (Figure S2). The Raman spectroscopy further reveals the structure of the Si shell. As shown in Figure 3e, the pristine Si/Cu NCA structures exhibit a broad peak centered at 480 cm^{-1} that is associated with amorphous Si and a thin band at 490 cm^{-1} that is the well-known nanocrystalline Si peak, which downshifted by ~30 cm^{-1} from that measured with single-crystalline Si(100) wafer. The position of the thin band directly depends on the cluster sizes and a growth of the crystallites provokes a blueshift of this band.[26,27] Thus, the shift was likely due to the much smaller crystal size and large disorders. The original Si shell likely consisted of nanocrystals embedded in an amorphous matrix associated with the feather-like TEM image in Figure 3b. The dominant amorphous structure of Si is also expected to lead to improved cyclic performance because amorphous Si has more favorable kinetics and fracture behavior when reacting with Li than does crystalline Si, making it a more desirable electrode active material.[28] After first charge-discharge tests, the sharp peak disappeared and merged into a single broad peak at 460 cm^{-1}. The bare Cu NCA sample did not show any feature in this range.

The electrochemical property and charge/discharge performance of the Si/Cu NCA structured electrode was evaluated in a three-electrode cell. Figure 4a shows the cyclic voltammogram (CV) curves of the first four cycles of the Si/Cu NCA electrode in the potential window between 0.01 V and 1 V vs Li^+/Li. The shape of the first cycling curve is essentially different from the subsequent ones. Only one cathodic peak at 0.08 V is observed in the first cycle, which can be assigned to the formation of $Li_{15}Si_4$ alloy.[29] During the first discharge process, broad and sharp peaks at 0.3 V and 0.46 V can be ascribed to the phase transition from Li_xSi alloy to Si. In the subsequent cycles, the CV curves almost overlap, indicating the excellent cycle performance of such Si/Cu NCA composite electrode. The peak currents at 0.08 V distinctly decrease from the first to the second cycle, while the peak potentials keep constant. Furthermore, a new reduction peak appears at 0.18 V. This change corresponds to the conversion of Si to Li_xSi alloy.

Figure 4c compares the cycling performance of 50CuSi, 70CuSi, 90CuSi (Here, 50,70 and 90 refer to the deposition time of 50 min, 70 min and 90 min, respectively.) electrodes at 1.5 C after initial activation at a low rate of 0.3 C in the voltage range 0.01–1.6 V vs Li^+/Li. First activation cycle with very low current helps to form stable SEI on the electrode surface, and to make active substances fully activated, thus, the battery will achieve the best capacity and performance. Furthermore, initial activation is important to avoid rapid capacity fading as a result of pulverization.[30] Both 50CuSi and 70CuSi electrodes exhibited superior cycle performance, up to 2000 cycles. The initial and final discharge capacities for the 50CuSi electrode were 1790 mAh g^{-1} and 1404 mAh g^{-1} , respectively, with a retention rate of 78.4 % (99.99% per cycle). The 70CuSi electrode yielded initial and final discharge capacities of 1445 mAh g^{-1} and 1006 mAh g^{-1}, respectively, and with a retention rate of 69.6 % (99.98% per cycle). In both cases, the capacities were much higher than reported 3D Si on Cu nanopillar electrodes.[14] Notably, a rise in capacity over the early cycles for 70CuSi electrode was observed, which was attributed to the activation process of electrode materials and side reaction from electrolyte. Similar phenomena have been reported in previous studies of Si-based anodes.[17,21,31] Coulombic efficiency (CE) is also an important evaluation criterion for silicon electrode. For 50CuSi and 70CuSi electrodes, the CE of the early cycles is low, but gradually increases in the following cycles, eventually stabilized at above 99%, which is much higher than other Si electrodes.[32-35] Still, it is possible to improve the CE by surface treatments and electrolyte modifications.[21] For comparison, the cycle performance of a planar 70CuSi electrode is shown in Figure S3. The discharge capacity of the planar electrode faded quickly, only 24.5% of initial capacity left after 100 cycles. The representative voltage profiles of the different cycles for 70CuSi electrodes are shown in Fig. 4b. The lithiation potential shows two sloping profiles between 0.2 and 0.01 V, consistent

with the behavior of CV curves. The electrode exhibits a reversible discharge capacity of 1445 mAh g^{-1} from the 1st cycle. This capacity experienced a sustained rise to a peak and then faded slightly during the following cycles (600th cycle: 1451 mAh g^{-1}, 800th cycle: 1369 mAh g^{-1}, 1000th cycle: 1290 mAh g^{-1}, 1200th cycle: 1238 mAh g^{-1}, 1500th cycle: 1133 mAh g^{-1}), indicating superior and stable cycling performance. However, fast capacity fading for 90CuSi anodes can be observed. The most likely explanation is that the space between each cylinder acting as the confining buffer was nearly swallowed by the increased Si layer thickness relative to the 50CuSi and 70CuSi electrodes (Figure 2f). In this case, stress is less able to relax, leading to poor cycle performance.

The morphological changes of Si/Cu NCA structures at first cycle were monitored by ex-situ TEM observation as a function of Li insertion concentration: i) at a charge voltage cutoff of 0.1 V, ii) after the full lithiation at 0.01 V, iii) after delithiation following the first cycle at 1.6 V. At the charge voltage cutoff of 0.1 V, with low lithium insertion concentration, and the resultantly limited volume expansion of silicon shell, the gaps between cones are filled up and core-shell structures are still clearly visible. The SAED pattern (Inset of Figure 5a) confirms that the Si shell maintains its amorphous structure. At the fully lithiated state, the Si shell volume further expanded, and the core-shell structure is no longer observable because the electron beam cannot transmit through the thick Si shell. The dispersed SAED pattern (Inset of Figure 5b) transformed into diffraction ring, revealing the formation of polycrystalline Li_xSi. This result is consistent with previous research.[4] In the process of lithium intercalation, amorphous silicon will be transformed into crystalline silicon at the critical potential. Also, better cycle performance will be achieved if silicon anodes are restricted to their fully amorphous range, above the critical potential, because high internal stresses appear in two-phase regions, which leads to particle cracking, poor electrical contact, and thus capacity fading. Figure 5c and 5d clearly show the volume changes of a single cone structured electrode during the first cycle by ex-situ TEM observation. The space between cones is effective in eliminating the stress caused by volume expansion. High magnification TEM image shows the Si layer after lithiation appears mesoporous (Figure S4).

Low power density is always the problem of LIB, despite the high energy density. Because of the limit of intrinsic diffusivity of the lithium ion in the solid state (ca. 10^{-8} cm^2 s^{-1}), it is nearly impossible to improve the rate of intercalation/deintercalation through the design of new materials, which inevitably limits charge/discharge rate.[37] Nanomaterials, however, have the genuine potential to improve the rate performance of lithium-ion batteries, as their reduced dimensions make far higher lithium insertion/removal rates possible. The reduced dimensions significantly increase the rate of lithium insertion/removal, because the characteristic time constant for diffusion is given by $t=L^2/D$, where L is the diffusion length and D the diffusion constant, the time t for intercalation decreases with the square of the diffusion length distances.[9] Figure 6a is the schematic illustration of electron transfer path of Si/Cu NCA structure and planar Si structure. Comparing with the planar electrode, Si/Cu NCA structured electrode has more contact area with the electrolyte and shortened diffusion distances of the ions and electrons, thus high charge/discharge rate.

In order to investigate rate performance of Si/Cu NCA electrodes, galvanostatic measurements were performed from 1.0 C to 25 C (1 C = 3580 mA g^{-1}). Figure 6b shows the discharge capacities of 50CuSi, 70CuSi, 90CuSi electrodes and planar 70CuSi electrodes at various current rates, which are 1.0 C, 1.5 C, 2.25 C, 2.75 C, 3.75 C, 5.5 C, 7.5 C, 11 C, 16.5 C, 25 C, and then back to the initial rate of 1.0 C. The 50CuSi electrode exhibited the best rate performance. The discharge specific capacities were 1898, 1915, 1898, 1904, 1898, 1838, 1761, 1623, 1426, and 916 mAh g^{-1} at the elevated rate, respectively, and then back to 2000 mAh g^{-1} at the rate of 1.0 C. The capacity increase when the rate returned to 1.0 C may be related to the activation of the unreacted inside region of silicon, which is generally accepted for Si anodes operated at high C-rate condition. The specific capacity of 916 mAh g^{-1} at 25 C is particularly noteworthy, because it has a capacity retention of 48.3% relative to the capacity at 1 C, and is 1.46 times higher than the theoretical capacity of graphite (372 mAh g^{-1}) at such rate. Remarkably, the 50CuSi electrode recovered to the discharge capacity of ~2000 mA h g^{-1} when the rate returns to 1.0 C from 25 C. For 70CuSi electrodes with a capacity of 1656.2 mAh g^{-1} at 1.0 C, the rate performance remains excellent and keeps a capacity retention of 25.6 % at 16.5 C. In comparison, the planar 70CuSi electrode exhibits a poor rate performance and a capacity retention of only 17.3% at 3.75 C. The 90CuSi electrode, with more active substance, demonstrates a lower rate performance, though still better than the planar electrode.

Silica-based electrodes, like germanium-based materials, also have been proven to have higher capacities at very high discharge rates if charged at a fixed, slower rate by previous studies.[31,36,38] In order to improve the discharge rate capability of the electrode, a representative 70CuSi electrode sample was charged at a fixed rate of 0.75 C while discharging from 1.5 C to 25 C (Figure 6c). The electrodes show a reduced capacity fade in the whole process. At 25 C, still a capacity of 1448 mAh g^{-1} (approximately 4 times that of commercial graphite) was maintained that is 80% of the initial discharge capacity at 1.5 C rate.

To explore the reason for such excellent cycle performance for the Si/Cu NCA structured electrode, cells were disassembled after 156 cycles and 3000 cycles (discharging up to 1.6 V) for SEM and TEM characterization of the electrode as shown in Figure 7. Compared with the image of the pristine sample, the morphology after cycling shows huge variation. After 156 cycles, the gaps between each cylinder disappeared and no obvious crevices can be seen (Figure 7a). In the process of charge-discharge, the gaps relieved the stress caused by continued expansion-shrinkage of Si electrode to form small coordinated regions randomly on the surface. The corresponding TEM image (Figure 7b) clearly shows Cu NCA

pierce into the Si coating tightly and therefore the coating is not shed off. After 3000 cycles, the Si layer looks more loose and porous, but still not peeling off (Figure 7c). The corresponding cross-sectional image proves the advantage of our well-engineered Si/Cu NCA structured electrode, the Cu NCA firmly grasp the silicon layer, even if the Si layers is very loose (Figure 7d, the white arrows).

Conclusions

In summary, we report a facile method for the successful preparation of silicon decorated Cu nanocone-array (NCA) for the application of lithium ion battery anodes. The Cu NCA current collector, the fabrication process of which is simple, low-cost, energy-efficient and eco-friendly, provides the advantages of high electric conductivity, robust structure support, and effective accommodation of strain. The Si/Cu NCA structured electrode exhibited excellent cycle stability up to 2000 cycles, high specific discharge capacity at 1.5 C and superhigh rate capability. These excellent performance metrics are attributed to the 3D core-shell nanostructure. Firstly, with free volume around the active material, stress is alleviated during the charge-discharge process. Secondly, such 3D nanoelectrodes increase electrode/electrolyte contact area, and shorten path lengths for electronic and Li^+ transport, thus improving the rate performance. Our results suggest the Si/Cu NCA structured electrode can be very promising for the manufacture of high cycle capability and high-power anode applications on a large scale.

Acknowledgements

This work is sponsored by National Natural Science foundation of China (No. 21303100) and Shanghai Natural Science Foundation (No. 13ZR1420400).

Notes and references

State Key Laboratory of Metal Matrix Composites, School of Material Science and Engineering, Shanghai Jiao Tong University, No. 800 Dongchuan Rd. Shanghai, 200240 PR China. E-mail: hangtao@sjtu.edu.cn; TEL: +86-21-3420-2748; FAX: +86-21-3420-2748

1 Maier, J., Nature materials 2005, 4, 805-815.
2 Armand, M.; Tarascon, J.-M., Nature 2008, 451, 652-657.
3 Poizot, P.; Laruelle, S.; Grugeon, S.; Dupont, L.; Tarascon, J., Nature 2000, 407, 496-499.
4 Obrovac, M.; Christensen, L., Electrochemical and Solid-State Letters 2004, 7, A93-A96.
5 Liu, B.; Soares, P.; Checkles, C.; Zhao, Y.; Yu, G., Nano letters 2013, 13, 3414-3419.
6 Wu, H.; Cui, Y., Nano Today 2012, 7, 414-429.
7 Zhang, X.-W.; Patil, P. K.; Wang, C.; Appleby, A. J.; Little, F. E.; Cocke, D. L., Journal of power sources 2004, 125, 206-213.
8 Aricò, A. S.; Bruce, P.; Scrosati, B.; Tarascon, J.-M.; Van Schalkwijk, W., Nature materials 2005, 4, 366-377.
9 Bruce, P. G.; Scrosati, B.; Tarascon, J. M., Angewandte Chemie International Edition 2008, 47, 2930-2946.
10 Cui, L.-F.; Ruffo, R.; Chan, C. K.; Peng, H.; Cui, Y., Nano Letters 2008, 9, 491-495.
11 Peng, K.; Jie, J.; Zhang, W.; Lee, S.-T., Applied Physics Letters 2008, 93, 033105.
12 Bang, B. M.; Kim, H.; Lee, J.-P.; Cho, J.; Park, S., Energy & Environmental Science 2011, 4, 3395-3399.
13 Föll, H.; Hartz, H.; Ossei‐Wusu, E.; Carstensen, J.; Riemenschneider, O., physica status solidi (RRL)-Rapid Research Letters 2010, 4, 4-6.
14 Kim, G.; Jeong, S.; Shin, J.-H.; Cho, J.; Lee, H., ACS nano 2014, 8, 1907-1912.
15 Cao, F. F.; Deng, J. W.; Xin, S.; Ji, H. X.; Schmidt, O. G.; Wan, L. J.; Guo, Y. G., Advanced Materials 2011, 23, 4415-4420.
16 YoubáKim, D.; WookáKim, D., Journal of Materials Chemistry A 2014, 2, 2478-2481.
17 Yao, Y.; McDowell, M. T.; Ryu, I.; Wu, H.; Liu, N.; Hu, L.; Nix, W. D.; Cui, Y., Nano Letters 2011, 11, 2949-2954.
18 Lee, B.-S.; Son, S.-B.; Park, K.-M.; Seo, J.-H.; Lee, S.-H.; Choi, I.-S.; Oh, K.-H.; Yu, W.-R., Journal of Power Sources 2012, 206, 267-273.
19 Liu, N.; Wu, H.; McDowell, M. T.; Yao, Y.; Wang, C.; Cui, Y., Nano letters 2012, 12, 3315-3321.
20 Song, T.; Cheng, H.; Choi, H.; Lee, J.-H.; Han, H.; Lee, D. H.; Yoo, D. S.; Kwon, M.-S.; Choi, J.-M.; Doo, S. G., Acs Nano 2011, 6, 303-309.
21 Wu, H.; Chan, G.; Choi, J. W.; Yao, Y.; McDowell, M. T.; Lee, S. W.; Jackson, A.; Yang, Y.; Hu, L.; Cui, Y., Nature nanotechnology 2012, 7, 310-315.
22 Jia, H.; Gao, P.; Yang, J.; Wang, J.; Nuli, Y.; Yang, Z., Advanced Energy Materials 2011, 1, 1036-1039.
23 Li, X.; Meduri, P.; Chen, X.; Qi, W.; Engelhard, M. H.; Xu, W.; Ding, F.; Xiao, J.; Wang, W.; Wang, C., Journal of Materials Chemistry 2012, 22, 11014-11017.
24 Taberna, P.-L.; Mitra, S.; Poizot, P.; Simon, P.; Tarascon, J.-M., Nature materials 2006, 5, 567-573.
25 Deng, Y.; Ling, H.; Feng, X.; Hang, T.; Li, M., CrystEngComm 2015, 17, 868-876.
26 Mallet, J.; Molinari, M.; Martineau, F.; Delavoie, F.; Fricoteaux, P.; Troyon, M., Nano letters 2008, 8, 3468-3474.
27 Klankowski, S. A.; Rojeski, R. A.; Cruden, B. A.; Liu, J.; Wu, J.; Li, J., Journal of Materials Chemistry A 2013, 1, 1055-1064.
28 McDowell, M. T.; Lee, S. W.; Harris, J. T.; Korgel, B. A.; Wang, C.; Nix, W. D.; Cui, Y., Nano letters 2013, 13, 758-764.
29 Zhou, X.; Wan, L. J.; Guo, Y. G., Small 2013, 9, 2684-2688.
30 Zhou, S.; Liu, X.; Wang, D., Nano letters 2010, 10 (3), 860-863.
31 Ko, M.; Chae, S.; Jeong, S.; Oh, P.; Cho, J., ACS nano 2014, 8, 8591-8599.
32 Szczech, J. R.; Jin, S., Energy & Environmental Science 2011, 4, 56-72.

33 Cho, J.-H.; Picraux, S. T.,Nano letters 2013, 13 (11), 5740-5747.
34 Song, T.; Cheng, H.; Town, K.; Park, H.; Black, R. W.; Lee, S.; Park, W. I.; Huang, Y.; Rogers, J. A.; Nazar, L. F., Advanced Functional Materials 2014, 24 (10), 1458-1464
35 Gowda, S. R.; Leela Mohana Reddy, A.; Zhan, X.;Ajayan, P. M., Nano letters 2011, 11 (8), 3329-3333.
36 Jung, D. S.; Hwang, T. H.; Park, S. B.; Choi, J. W., Nano letters 2013, 13, 2092-2097.
37 Xin, S.; Guo, Y.-G.; Wan, L.-J.,Accounts of chemical research 2012, 45, 1759-1769.
38 Kennedy, T.; Mullane, E.; Geaney, H.; Osiak, M.; O'Dwyer, C.; Ryan, K. M., Nano letters 2014, 14, 716-723.

Figure list

Figure 1 Schemetic illustration of the fabrication process of a copper nanocone-array supported silicon anode architecture: (a) the plating bath used for the fabrication of the nanostructure Cu current collector, (b) Copper nanocone-array before Si coating, (c) after Si coating. This electrode requires no binder or conductive additive for use as an electrode in LIBs.

Figure 2 (a) Low magnification and (b) high magnification SEM images of Cu NCA. (c-f) Si-based nanostructured 3D electrode for several magnetron sputtering deposition times (c, 25 min; d, 50 min; e, 70 min; f, 90 min).

Figure 3 (a) the low magnification TEM image and (b) the high magnification TEM image of Si/Cu NCA structures. (c) The Selected Area Electron Diffraction pattern (SAED) recorded over a single Si/Cu NCA structures (d) A high-resolution TEM image at the interface of the black core and gray shell. (e) Raman spectra of a bare Cu NCA (red line) and a Si-coated Cu NCA before (purple line) and after (green line) charge–discharge cycling compared to the reference using a Si (100) wafer (black dashed line).The measurements were recorded with a Raman microscope with 532 nm laser at 20 mW power.

Figure 4 (a) CV curves of the first four cycles of Si/Cu NCA electrode. (b) The representative voltage profiles of the different cycles for 70CuSi electrodes (c) Cycling performance of 50CuSi, 70CuSi and 90CuSi electrodes at 1.5C after initial activation of low current in the voltage range 0.01-1.6 V vs Li^+ /Li.

Figure 5 Ex-situ experiments of Si/Cu NCA structures after cycling at 1.5C and different low voltage cutoffs at the first cycle. (a) TEM and SAED (inset) image of Si/Cu NCA structures with cutoff of 100 mV. (b) TEM and SAED (inset) images of Si/Cu NCA structures with cutoff of 10 mV. (c) TEM image of a single cone structure after lithiation. (d) TEM image of a single cone structure after delithiation.

Figure 6 (a) Schematic illustration of electron transfer path of Si/Cu NCA structure and planar Si structure. (b) Discharge capacities of 50CuSi, 70CuSi, 90CuSi electrodes and planar 70CuSi electrodes at various current rates (1 C = 3580 mA g^{-1}). (c) The discharge capacities measured for 40 cycles at 1.5C and 5 cycles at the other 8 different discharge rates are shown. The charge rate was kept constant at 0.75C for all cycles.

Figure 7 Electrode morphology change before and after cycling. (a) SEM images and (b) TEM images of Si/Cu NCA structured electrode after 156 cycles. (c) Top-view SEM image and (d) Cross-sectional SEM images SEM images after 3000 cycles.

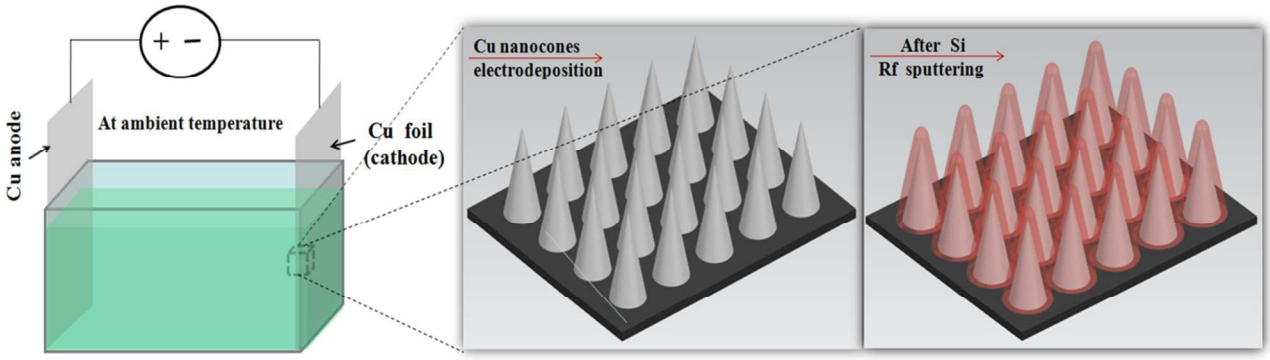

Figure 1

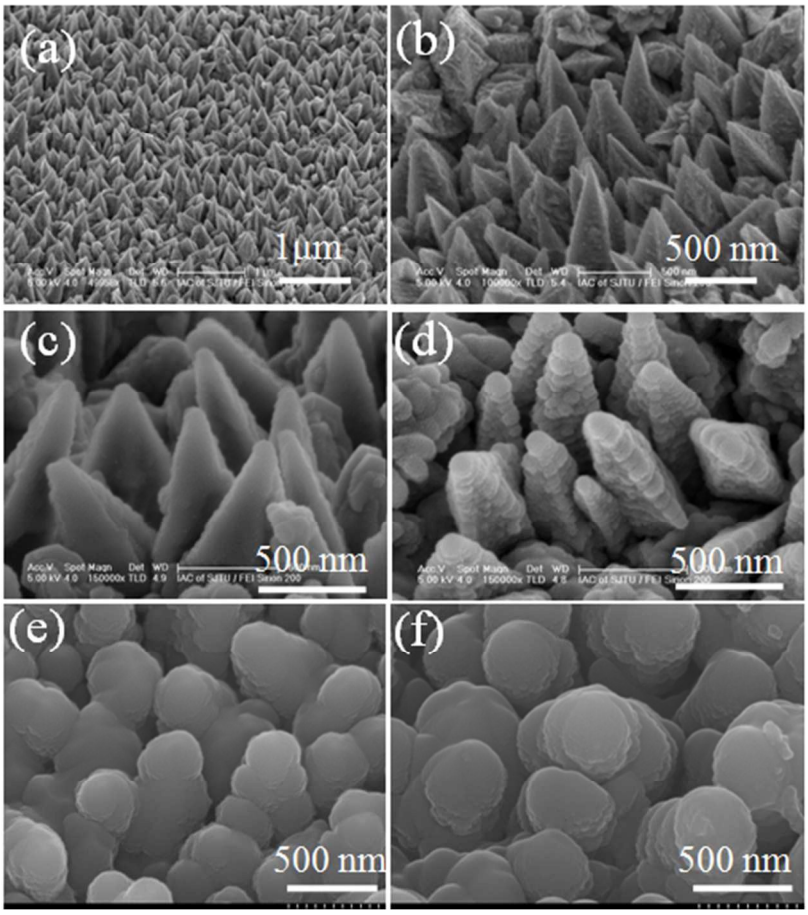

Figure 2

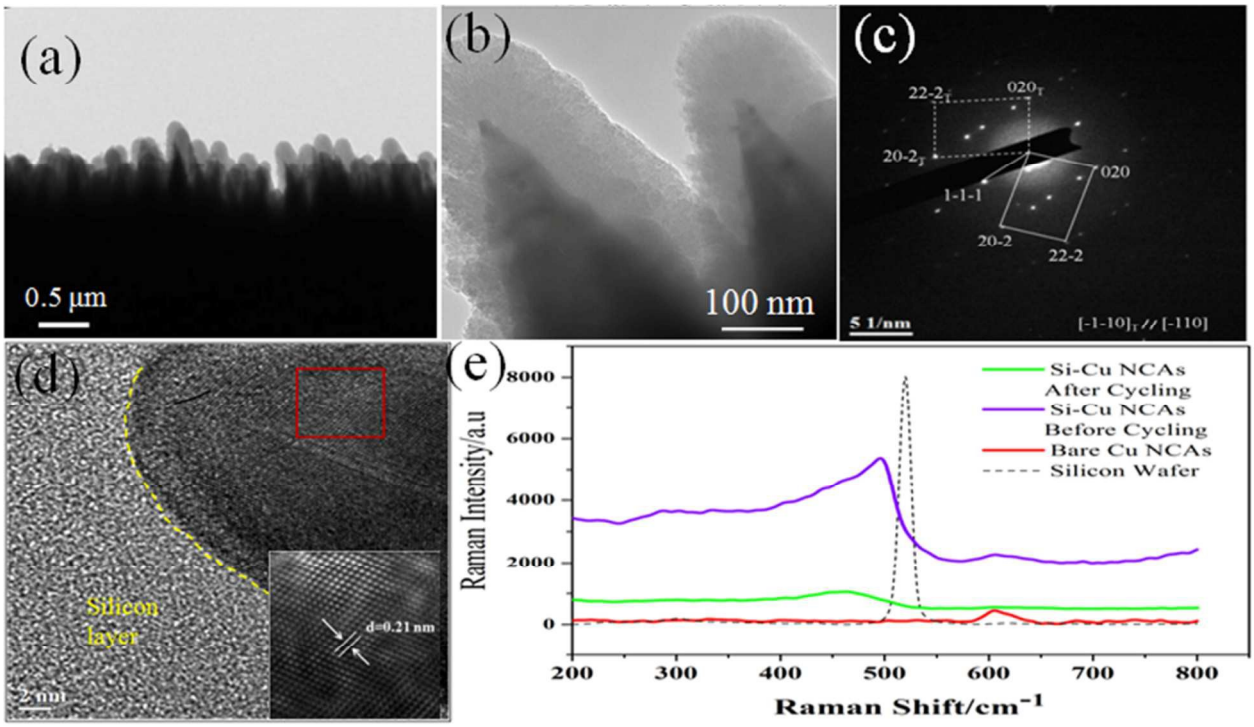

Figure 3

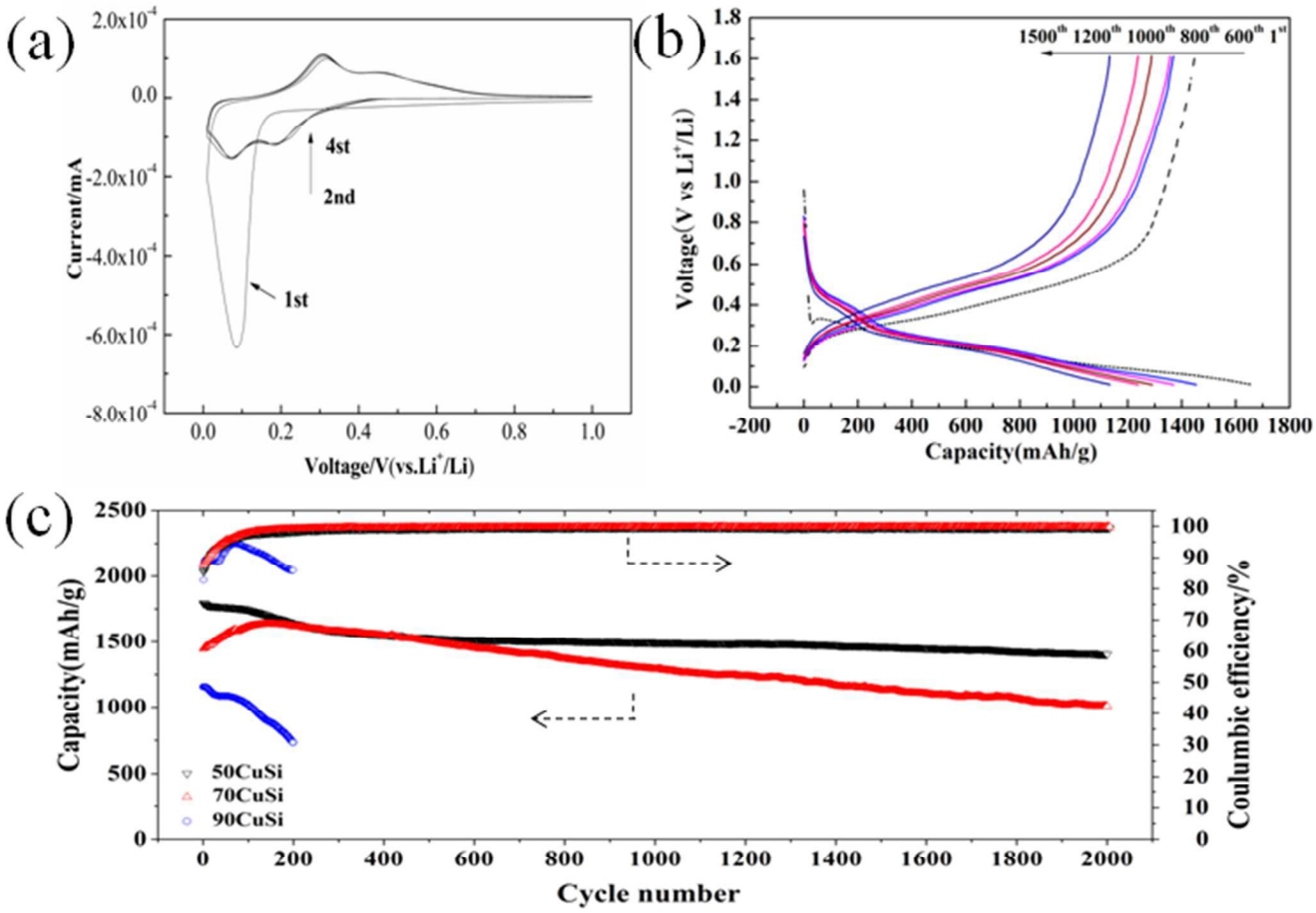

Figure 4

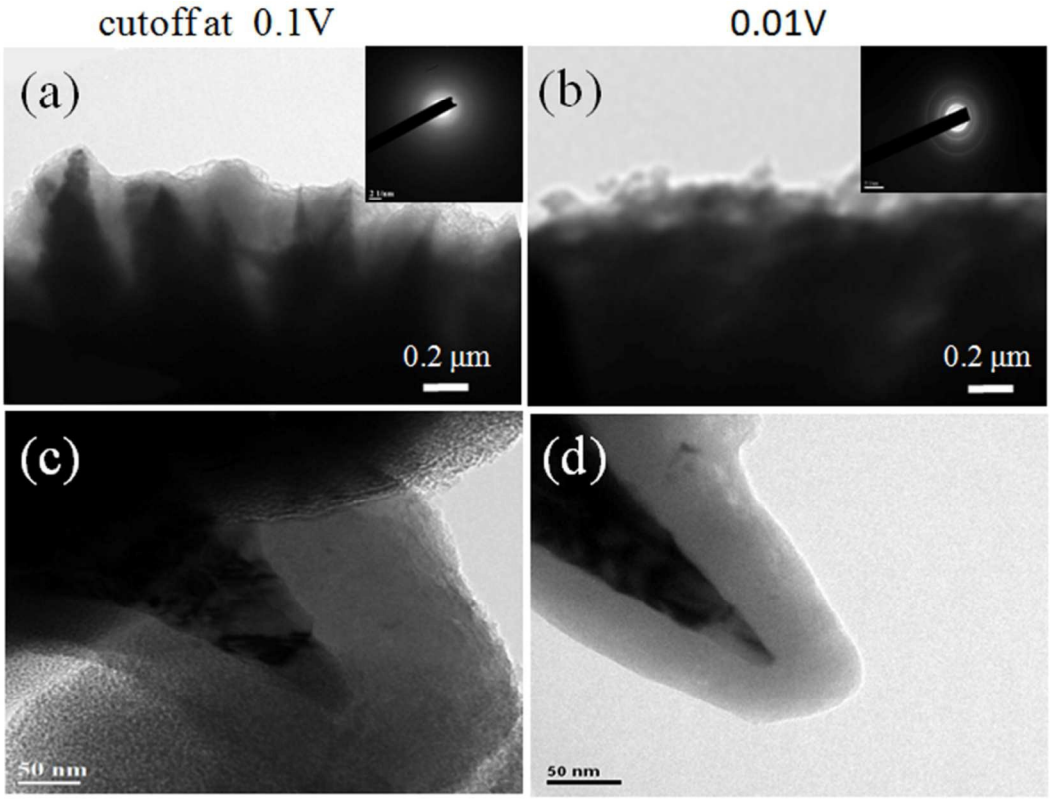

Figure 5

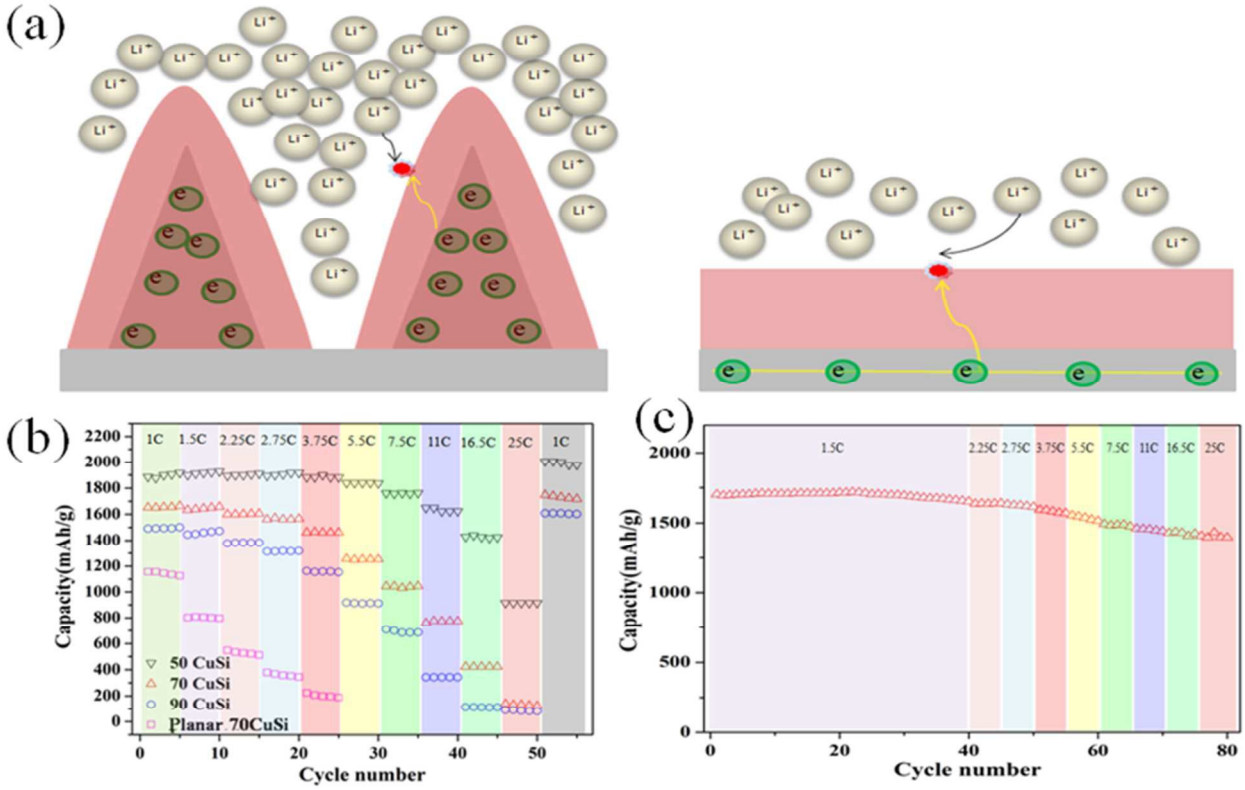

Figure 6

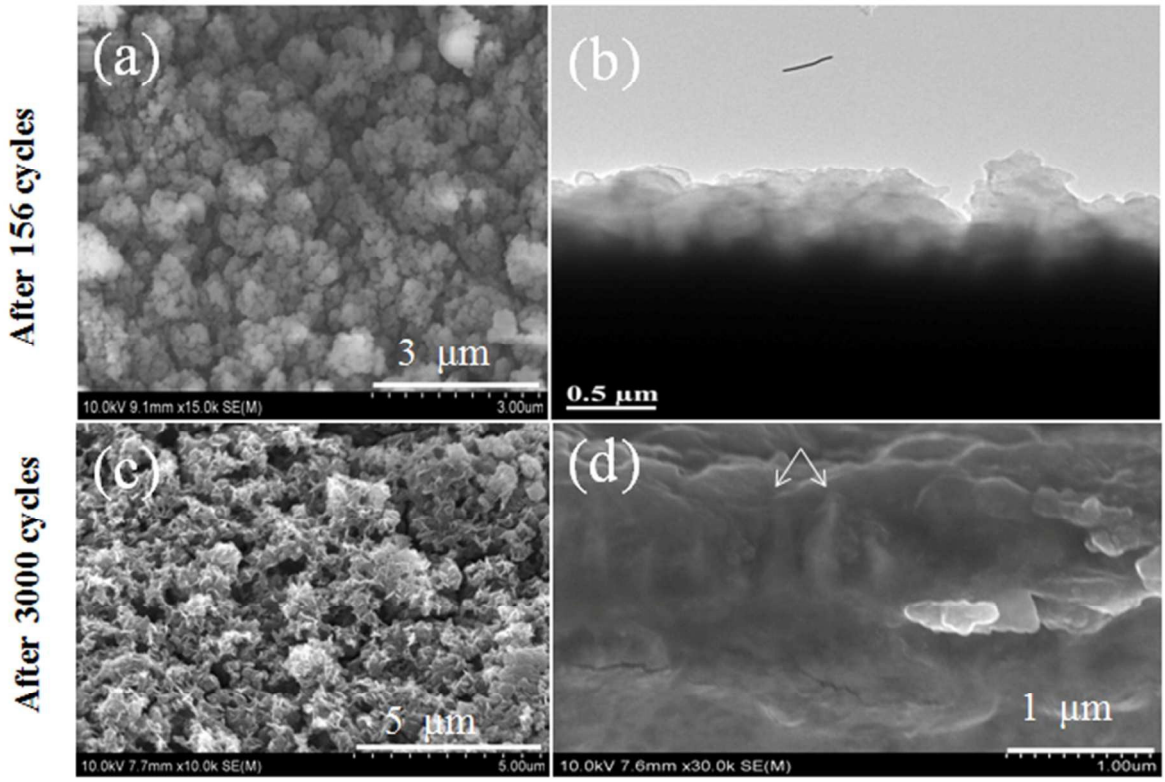

Figure 7

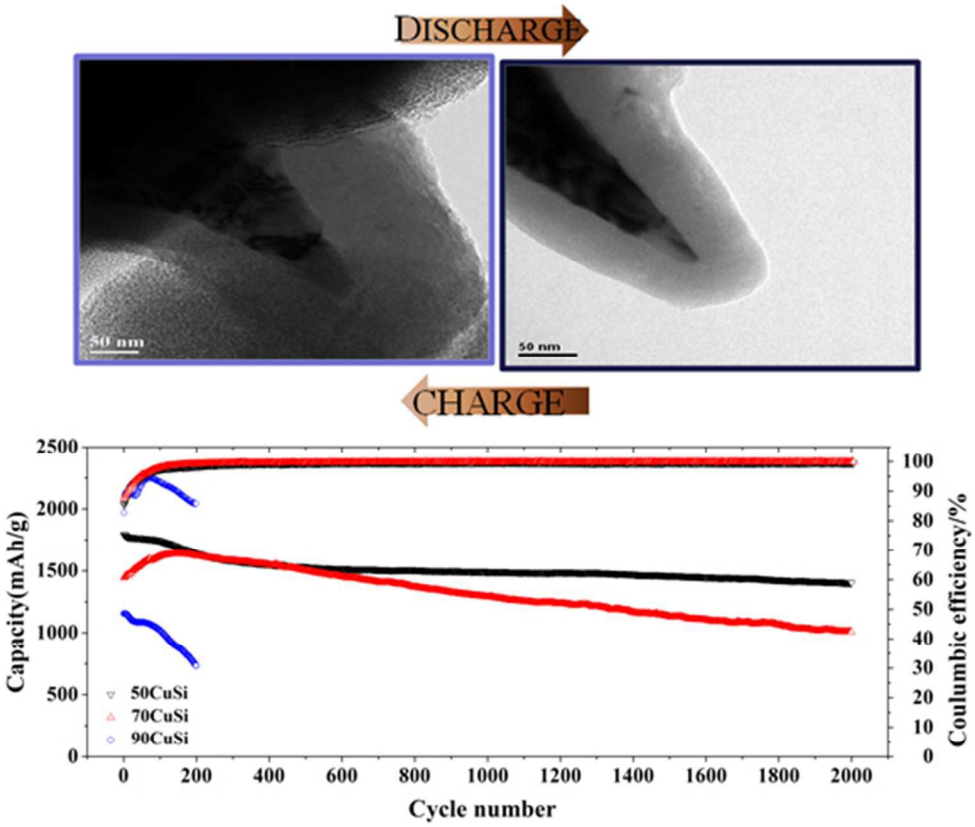

157x135mm (96 x 96 DPI)